R 01-17

A01-29275

AIAA 2001-2021

Inflation and Glide Studies of Slider-Reefed Cruciform Parachutes

J. Potvin[1], G. Peek[2], B. Brocato[3], T. Perschbacher[5] and R. Kutz[3]
Parks College Parachute Research Group
Saint Louis University, St. Louis, MO 63103

R. J. Benney[4]
U.S. Army Soldier and Biological Chemical Command
Natick Soldier Center
Natick, MA, 01760

Abstract

This two-part study is aimed at testing the performance of slider reefing on cruciform parachutes deployed in cargo airdrop environments, and at evaluating their glide and turn performance when flown with selected suspension lines trimmed to various lengths. The results of the inflation study include both numerical simulations and experimental data, calculated for, or collected from half-scale and full-scale cruciform parachute drops involving sliders. We also present the preliminary results of a series of inflation studies performed on a slider-reefed parachute outfitted with an additional reefing line routed around its crown area. In the second part of the paper we discuss the results of wind tunnel tests performed on $1/8^{th}$ –scale models trimmed for several glide configurations, and briefly discuss the details of upcoming radio-controlled test flights of a full-scale cruciform parachute system.

[1]Associate Professor, Department of Physics, member AIAA
[2]Consultant, Industrologic Inc.
[3]Student Member AIAA
[4]Aerospace Engineer, Senior Member AIAA
[5]Undergraduate Research Assistant

Introduction

The need for accurate cargo airdrop operations carried out from a high altitude and/or large offset has lead to the development and commercialization of several self-guiding parachutes systems. Based on the use of parafoils, these systems have integrated an on-board personal computer, a GPS unit and line pulling winches for autonomous flight control [1, 2]. Recently, the desire for fielding a cheaper self-gliding system has motivated the U.S. Army into funding further research, this time on the application of such GNC technology to C-9 and G-12 flat circular parachutes [3 - 7]. To compensate for the parachutes' well-known lower gliding performance, the effort has included the implementation of a vastly improved capability for wind prediction over the drop zone, to be integrated on a computer-based release point calculation platform [6]. In this paper we discuss the application of this technology to cruciform parachutes, which represents yet a cheaper alternative. We report on a study of the inflation performance of slider reefing on cruciform parachutes, using data obtained from both computer simulations and test drops. We also present the first results of our investigation of the glide and turn performance of cruciform parachutes flown with selected suspension lines trimmed to various lengths. This study was accomplished via the measurement of the transverse force exerted on cruciform parachutes trimmed in a gliding configuration using wind tunnel experimentation on a $1/8^{th}$-scale model.

Inflation Characteristics

The inflation characteristics of cruciform parachutes have been studied for a long time [8]. Like any other parachutes of small-to-moderate geometric porosity, cross chutes may open fast and hard when deployed at high speed without the use of opening shock control devices such as skirt-line reefing (figure 1). Of immediate interest to us was the possibility of using slider reefing, which has the potential of being as effective as line reefing but much cheaper.

Slider-reefed cruciform parachute inflation proceeds in stages that are similar to the inflation of slider-reefed ram-air parachutes [9, 10]. After line stretch and while in a "slider up" configuration, the parachute inflates to several intermediate and temporary shapes (figure 2). On most slider-reefed round and cruciform parachutes, this "early pressurization" phase features the largest opening loads. This phase is then followed by the so-called "slider descent" or "canopy spreading" phase, were the inflated shape of the canopy generates a line tension differential below and above the slider that is high enough to push the slider down the suspension lines (figure 2).

Test drops

A series of 53 drops were carried out in 1999 and 2000 with the purpose of evaluating the opening characteristics of cross chutes outfitted with simple sliders. The test drops were carried out at 1000 feet MSL in the St. Louis MO area, from aircraft flying at speeds ranging between 90 and 110 KIAS. The payloads consisted of 100 - 300 lbs steel tubs (nearly) shaped as half-scale models of the U.S. Army A-22 container, with dimensions of 24in x 20in x 23in (figure 3). Each tub was instrumented with a load cell inserted on each of the two parachute risers (figure 4), and with an electronic barograph located inside the tub. These instruments sent data to an on-board data acquisition system recording at a rate of 500 Hz. All components were built using off-the-shelf components [11-13]. The parachute tested were constructed as follows (figure 5):

- A one-of-a-kind U.S. Army-Natick-designed 24ft cruciform parachute, built out of two 9.2ft-by-24.0ft panels sewn into a cross and attached to 20 suspension lines of length 19.7 ft. The cloth had a permeability of 30 to 45 cfm and was made of 200 denier nylon; the suspension lines were made of MIL-C-7515 Type V chord.
- Half-scale models of this U.S. Army cruciform parachute, built out of two 4.2ft-by-10.7ft panels and 20 suspension lines of length 12.2 ft and 17.0ft. The cloth used was the same as for the full- scale article and the suspension lines were of MIL-C-7515 Type I-A chord.

The terminal speed of these cruciform chutes was measured at about 17.8 ft/sec and 32 ft/sec while carrying payloads of 100 and 128 lbs respectively.

The sliders used in this study were initially of circular shape and mounted in a foldable frame to insure correct shape at line stretch (figure 6). As the initial testing showed such frames to be superfluous, a basic rectangular design made of nylon tape and fabric was adopted (figure 7), and made in several sizes (See Tables 1-3). These sliders were built in a manner identical to those used on skydiving ram-air parachutes. A crucial design feature was the presence of a vent hole to allow a limited but unobstructed airflow inside the parachute when in the "slider up" configuration. In this regard, we followed the example of slider designs used on current commercial cupped parachute systems, such as the Sombrero slider [14] or the BRS slider [15]. Without a vent hole of at least 10% area (w/r to total slider surface area), very little inflation is accomplished in the first 10 to 20 seconds of freefall, which would constitute an unacceptable delay in low altitude air drops.

Some of the test drop results are summarized in Table 4, which includes comparisons between the maximum opening forces measured on parachutes outfitted with sliders and parachutes that did not. At the half scale level, the use of sliders contributed to up to a 50% reduction in opening shock as can be seen by comparing figures 1 and 8. This trend is repeated at full scale and similar wing loading. Almost no reduction is seen at the full-scale level but very low wing loading.

Double reefing tests

Further opening shock reduction of slider-reefed systems can be achieved by adding line reefing (figure 9). One advantage is that such system is effectively doubly reefed, and yet involves only

one pyrotechnic cutter. Moreover, this arrangement has the advantage of providing a drogue flight mode capability without the addition of a drogue chute and associated deployment hardware [16].

With regards to inflation, using a reefing line routed around the parachute's crown (see definition in figure 5) and cut by a timed pyrotechnic device was found to yield an extra inflation stage which provided further speed reduction and lower opening shocks. As shown in figure 9, our design involved setting the reefing line circumference to a small enough length to yield a partially inflated canopy that generates too small of a line tension differential around the slider to cause its descent down the suspension lines. With such design slider descent would be initiated only upon the activation of the reefing line cutter, which would then allow full canopy inflation in the slider- reefing mode (figure 9). Our tests have shown that a reefing line circumference of about half of the slider's circumference would produce a partially inflated shape that yielded a good enough speed reduction and the least parachute apex oscillations during the drogue phase.

Inflation modeling

Simulating the inflation of slider-reefed cruciform (and also flat circular) parachutes involves the separate modeling of the two inflation stages, i.e. early pressurization and slider descent. (The inflation of double reefing will not be discussed further in this paper). A third stage needs to be included as well, namely the post-inflation deceleration phase, during which the parachute completes its transition from the horizontal to the vertical while fully inflated, in order to further decelerate into its steady descent rate regime (i.e. terminal velocity).

The modeling of the trajectory of an inflating and post-inflating parachute is based on the combined parachute/load Newtonian equation of motion, here written for a purely vertical trajectory for the sake of simplicity:

$$ma(t) = -\frac{1}{2}\rho\Sigma(t)v^2(t) + W \qquad (1)$$

where parameters m, a, v, ρ and W correspond to the system's total mass, deceleration, descent speed, air density at deployment altitude and system total weight respectively. However, such an equation cannot be solved until the time dependence of the drag area, i.e. $\Sigma(t) \equiv C_D(t)S(t)$, is known. Such information depends on the aerodynamics and physics of the specific inflation phase under consideration.

- Early pressurization

Early pressurization takes place after the suspension lines have deployed and stretched, and after the parachute has been pulled out of the bag. Early pressurization begins when the parachute adopts a tube-like shape and ends when it has an inverted pear-like shape (Figure 2). Lengthening the duration of early pressurization is one sure way to reduce opening shock since even a partly opened parachute will generate enough drag to cause a substantial deceleration of the payload.

The simulation model used for this stage is Ludtke's well-tested formalism, which describes the inflation of many *unreefed* parachute shapes of small geometric porosity [8, 17]. Here we are assuming that the model can perform as accurately for a parachute which evolves from a tube into an inverted pear (see figure 2). Crucial to our assumption is the fact that this inflation process would proceed *unimpeded*, that is, without the use of hardware aimed at slowing down the evolution of the tube into the inverted pear.

Ludtke's formulation is based on the t^6-law applying to the parachute's drag area, namely:

$$\Sigma(t) = \left[\frac{C_D(t_{final})S(t_{final}) - C_D(0)S(0)}{t_{final}^6}\right] t^6 + C_D(0)S(0) \qquad (2)$$

Ludtke's formulation requires the empirical knowledge of the early pressurization duration (t_{ep}) which we get from from the measured riser load data. Also needed is the initial tube drag area, here estimated at $C_D S \sim 4.0\ ft^2$ (full-scale), and the final inverted pear-shape drag area, which was estimated at $C_D S \sim 80\ ft^2$ (full-scale).

- Slider descent – canopy spreading

The inflation of slider-reefed parachutes during the canopy spreading phase can be described by the Ideal Parachute Model [9, 10, 19], which supplements (1) with a drag area differential

equation derived from the slider's own Newtonian equation of motion. Along a vertical trajectory this extra drag area equation would be as follows:

$$\frac{d^2\Sigma}{dt^2} = \left[(K_1 + K_2\Sigma(t)) + (K_a + K_b\Sigma^{1/2}(t) + K_c\Sigma^{3/2}(t))\right]v^2(t) \quad (3)$$

The K-factors are known constants or functions of time written in terms of a parachute's specific construction characteristics. These factors would have the following property [9]:

$K_1, K_2 \neq 0$ & $K_a, K_b, K_c = 0$ for ram-air parachutes, and $K_1, K_2 = 0$ & $K_a, K_b, K_c \neq 0$ for round, cruciform or other symmetrically cupped parachutes. They can be directly related to a parachute's initial drag area, final drag area, suspended weight, descent velocity prior to slider descent down the suspension lines and suspension line lengths. They also depend on the slider construction characteristics such as weight and surface area.

Equation (3) can be approximated to a far simpler form, given that the shapes adopted by our test parachutes showed little changes in the forward-projected surface area during slider descent (see figure 2). Moreover, we argue that the change of $C_D(t)$ is small compared to the change in v^2 during this inflation stage [10]. This would lead to:

$$\frac{d^2\Sigma}{dt^2} \approx \Gamma v^2(t) \quad (4)$$

where Γ is a constant. In this respect equation (4) is very similar to the drag area evolution law used on small ram-air canopies [10]. The difference resides in the size-scaling properties of Γ, which for (small) cupped parachutes is far less sensitive to size than for ram-air parachutes.

- Post-inflation deceleration

Following swift inflation, the deceleration of fully opened parachutes rarely takes place at constant drag coefficient. The reason is that a significant amount of air near the parachute (or "added mass") co-decelerates along with the parachute-payload system, thus effectively changing the inertia of the latter [18, 20-24].

Formulations based on added mass have been used with mixed results, depending on the specific parachute application. Recently, some of us have proposed a new and more general drag coefficient formula which, in principle, can be applied to all (subsonic) parachute problems. It is based on the Galilean equivalence between bodies decelerating in a static fluid and those drifting with a moving fluid *and* accelerating to the speed of the fluid. Such equivalence, together with the assumption of an acceleration-independent $C_D(t)$ yields the following result [18]:

$$C_D(t) = C_D^{init}\left(\frac{v(t)}{v_I}\right)^{\beta'-2} \quad (5)$$

where

$$\beta' = 2 + \frac{\ln\left(\frac{C_D^{init}}{C_D^{steady}}\right)}{\ln\left(\frac{v_I}{v_T}\right)} \quad (6)$$

Here v_I, v_T, C_D^{init} and C_D^{steady} would correspond to the speed at the beginning of post-inflation, the system's terminal speed, the drag coefficient at the beginning of post-inflation and the steady state drag coefficient reached at the end of deceleration, respectively. In other words, this result would imply that the drag coefficient of similar objects may not be the same, depending on the initial and final conditions descent rates and drag coefficients. Examples and a full discussion of this fact can be found in reference [18, 24].

Non-vertical trajectories

Being launched from a moving aircraft, our test parachutes begin to inflate soon after clearing the aircraft door. This requires the simulation to account for a non-vertical trajectory though the use of the following equation and substitution in (1) [20]:

$$\frac{d\theta}{dt} = -g\frac{\sin\theta}{|v|} \quad (7)$$

$$W \rightarrow W\cos\theta(t) \quad (8)$$

Note that equation (1) neglects the elastic response of the suspension lines and parachute cloth during inflation, which for the light payload weight used in our tests allows the full transmission of the drag force to the load measuring cells in a time scale much shorter than the inflation time.

Comparing simulations with experiment

A first series of simulations and comparisons with test drop data was carried out to test the idea of using Ludtke's t^6-law to simulate the early pressurization phase. In particular, we used the data generated during drops NWV114 and NWV116, which involved the use of the full-scale parachutes carrying a 110 lbs payload. In these two cases, the slider had a very high drag area and traveled over a very short distance down the suspended lines. In other words, the parachute (partially) inflated *without a slider descent phase*. For this reason, most of the high drag forces sustained occurred during early pressurization and post-inflation. Simulating these two drops via the use of equations (1), (2), (5) – (8) gave the calculated forces shown in figure 10, graphed along with the measured riser forces. Theory and data appear to agree nicely.

Simulations of inflation sequences involving all three stages and using (1), (2), (4) - (8) are shown in figures 11 - 13. Again the comparison with experiment shows a good match. Besides the empirical estimates needed in Ludtke's model (early pressurization), the value of the initial speed was tuned to give the best drag force at t = 0. Also, the value of the drag area rate constant was estimated at $\Gamma \sim 1$, based on the slider Newtonian equation of motion from which it is derived. All other input parameters were calculated form the knowledge of the parachute characteristics and drop conditions.

Figures 11 – 13 feature arrows that show the beginning of the each inflation stage, as well as the beginning of post-inflation. It is interesting to note the contrast of drag force profiles between slider reefed systems with those of unreefed systems (see for example reference 24). In the former, most of the drag decrease appears to occur during the slider descent stage. In the latter it occurs during post-inflation. Moreover, the post-inflation stage with slider reefing seems to be characterized by a regime of constant drag coefficient, again in contrast with some unreefed parachute systems.

Gliding Characteristics

Like round parachutes, cruciform parachutes can be made to glide and turn via the pulling of certain suspension lines, i.e. generating motion on the side of pulled lines or motion opposite to the side of lengthened lines. Of most interest to us were the combinations of pulled/lengthened lines that allowed the cross to fly in an "X" configuration rather than in a "+" configuration. These combinations would thus allow, at least in theory, to fly at fast forward speeds without the nose-tuck that is often noticed on gliding round parachutes.

A series of wind tunnel runs at the Saint Louis University 3 ½ -by-3 ½ subsonic wind tunnel using a 1/8th parachute model was conducted to measure the transverse-force-over-drag ratio, or F_{transv}/F_D . Most of the hardware used in this experiment was similar to that discussed in references 25 and 26, including the use of the following equipment: a parachute model built out of two 3ft-by-1ft panels (zero-fabric permeability) and 51in suspension lines; and a load cell located at the suspension line confluence point to measure overall drag. One new feature was the use of an additional load cell to measure the transverse force that would be generated when the model is in a glide configuration. The load cell was linked to the parachute's apex and to the tunnel wall by nylon line that made a 90-degree angle with the main axis of the parachute-suspension line system. Although the separate measurement of F_{transv} and F_D are be subject to model-induced tunnel blockage effects [25], we expect the ratio F_{transv}/F_D to be less sensitive to this type of systematic error.

The specific line bias configurations that were studied are shown in figure 14. Tables 5 – 9 summarize the results obtained for one of the many speed values considered. These results suggest the best force ratios to be in the 10% range. However, being obtained under infinite mass conditions means that this result remains to be confirmed by further testing, in particular, flight testing. It is anticipated that under free flight conditions both vectors F_{transv} and F_D would remain orthogonal but become titled according to the glide slope.

Upcoming R/C Flight Testing

The coming months will see the execution of several test drops, to be performed with full-scale cross chutes trimmed with two inner lines pulled to a shorter length on the front side of the parachute, and with two inner lines trimmed to variable lengths on the back side (see configuration 3 in figure 14). This kind of trim would allow the parachute to go forward (lengthened back-side lines) as well as backward (pulled back-side lines), or to initiate turns (one back-side line pulled or lengthened). The flight of this parachute-payload system is to be ground-controlled by a R/C unit enabling line- pulling or lengthening by a set of two winches. As in the tests performed on the AGAS system [3, 4], the payload will also include a GPS unit for the tracking of its trajectory. This GPS data is to be compared with the GPS data of a separate non-gliding parachute dropped at the same time (and at the same descent rate), for the purpose of subtracting out the influence of the wind on the trajectory. The results of these tests are to be compared with our wind tunnel tests. They are to demonstrate also the feasibility of using gliding cross chutes for a self-guided, accurate cargo airdrops.

Acknowledgments

This work was supported by the US Army Soldier, Biological and Chemical Command (SBCCOM) under contract DAAD16-00-C-9250, and by the US Air Force Office of Scientific Research (AFOSR) under grant F49620-98-1-0125. The authors thank C. Lee and S. Patel (SBCCOM-Natick, MA) and S. Walker (AFOSR) for their advice and support. We also thank J. T. Blimling, R. Eddy, J. Gentry, O. Guerrero, C. Loehner, J. Mark, J. Papke, and T. Poston for their help during the experimental phase of the project. We finally thank Mr. T. Hawthorne for his help during the preparation of the manuscript.

References

1. Wailes, W. K. and Harrington, N. E.; "The Guided Parafoil Delivery System Program"; AIAA- 95-1538; *13th AIAA Aerodynamic Decelerator Systems Technology Conference*, Clearwater Beach, FL, 1995.

2. Geiger, R. H. , Smith , J. , and Stewart, S. M.; "Development of the Pioneer GS-750-1 Parafoil"; AIAA-95-1586; *13th AIAA Aerodynamic Decelerator Systems Technology Conference*, Clearwater Beach, FL, 1995.

3. Brown, G., Haggard , R. and Benney, R.; "A New Pneumatic Actuator: Its Use in Airdrop Applications"; AIAA-99-1719; 15th CEAS/AIAA Decelerator Systems Technology Conference which took place in Toulouse, France, 8-11 June 1999.

4. Brown, G. , Haggard, R., Almassy, R. and Benney, R. ; "The Affordable Guided Airdrop System (AGAS)"; AIAA-99-1742; 15th CEAS/AIAA Decelerator Systems Technology Conference which took place in Toulouse, France, 8-11 June 1999.

5. Dobrokhodov, V., Yakimenko, O., Kaminer, I., Howard, R., Dellicker ,S., Benney, R.; "Development and Flight Testing of the Affordable Guided Airdrop System for G-12 Cargo Parachute; presented at this conference.

6. Hattis, P., Benney, R., Fill, T., Rubenstein, D. and Wright, R.; "Status of an On-Board PC-Based Airdrop Planner Demonstration "; presented at this conference.

7. Pena, B. and Kelly, K.; "Wind Study and GPS dropsonde applicability to airdrop testing"; presented at this conference.

8. Knacke, T.W.; "Parachute Recovery Systems Design Manual"; Para Publishing, Santa Barbara CA 1992.

9.Perschbacher, T. and Potvin, J.; "The Improved Ideal Parachute Model and its Application to the Study of Inflation Dynamics of Slider-Reefed Ram-Air and Round Parachutes"; 15th CEAS/AIAA Decelerator Systems Technology Conference which took place in Toulouse, France, 8-11 June 1999. AIAA Paper-99-1750.

10. Potvin, J., Brocato, B. and Peek, G. "Modeling the Inflation of Ram-Air Parachutes Reefed with Sliders"; to appear in *Journal of Aircraft.*

11. Potvin, J., Montanez, R. and Peek, G.; "The Parks College Ram-Air Parachute Deployment

Study: a Status Report". AIAA-97-1426; *14th AIAA Aerodynamic Decelerator Systems Conference and Seminar*, San Francisco CA, June 1997.

12. Potvin, J., Montanez, R. and Peek, G.; "The Parks College Ram-Air Parachute Deployment Study". Proceedings of the *1997 Parachute Industry Association International Symposium*, Houston, TX, February 9-13, 1997.

13. Potvin, J., and Peek, G.; "The Parks College Parachute Research Group: Putting Science at the Service of Riggers and Manufacturers"; Proceedings of the *1999 Parachute Industry Association International Symposium*, San Diego, CA, January 10-14, 1999.

14. Butler, M.; Design, Development and Testing of Parachutes Using the BAT Sombrero Slider", *15th CEAS/AIAA Aerodynamic Decelerator Systems Technology Conference and Seminar*, Toulouse, France, June 1999. AIAA-99-1708.

15. See for example the press release appearing in Flying Magazine, October 1998.

16. R. Benney, S. Patel, G. Peek, J. Potvin; patent pending.

17. Ludtke, W. P., "A Technique for the Calculation fo the Opening-Shock Forces for Several Types of solid Cloth Parachutes", AIAA-73-477. *4th AIAA Aerodynamic Decelerator Systems Technology Conference*, Palm Springs, CA, 1973; pp. 176 – 185.

18. Potvin, J., Peek, G., and Brocato, B.; "Using Galilean Relativity for the Study of Unsteady Drag"; December 2000. Submitted for publication.

19. Potvin, J.; "Testing a New Model of Ram-Air Parachute Inflation"; *The Aeronautical Journal*, **101**, pp. 299-313, 1997. Erratum: Figure 4b should be plotted versus $-\ln(t_{max}\, g/v_0)$ rather than $\ln(t_{max}\, g/v_0)$ as claimed; also, equation (17) is incorrect and should read:

$$R_f = t_f g / v_0$$
$$= 2 g \Sigma_0^{1/4} (\sqrt{\Sigma_f} - \sqrt{\Sigma_0})^{1/2} / v_0^2 K$$

20. Lingard, J. S. "The Effects of Added Mass on Parachute Inflation Force Coefficients"; AIAA-95-1561. *13th AIAA Aerodynamic Decelerator Systems Technology Conference*, Clearwater Beach, FL, 1995; pp. 176 – 185.

21. Wolf, D., E., "A Simplified Dynamic Model of Parachute Inflation", *Journal of Aircraft*, **11**, pp. 28-33, 1974.

22. Sarpkaya, T. and Isaacson, M., *Mechanics of Wave Forces on Offshore Structures"*, Van Nostrand Reinhold Company, New York, 1981.

23. Sarpkaya, T., "Method of Analysis for Flow Around Parachute Canopies", *11th AIAA Aerodynamic Decelerator Systems Technology Conference*, AIAA, Reston, VA, 1991, pp. 1 – 17 ; AIAA Paper 91-0825.

24. Potvin, J., Peek, G., Brocato, B., Kutz, R., Manglano, C. and Yavitz, B.; "Deceleration Dynamics of Cruciform and Flat Circular Parachutes During and After Inflation: A Drag Coefficient Time Dependence Study"; see paper AIAA-2000-2028 presented at this conference.

25. Potvin, J., Esteve, Peek, G., Alamat, R., and Little, J.; "Wind Tunnel Study of Cruciform Parachutes Folded in Various Configurations"; 15th CEAS/AIAA Decelerator Systems Technology Conference which took place in Toulouse, France, 8-11 June 1999. AIAA Paper-99-1739.

26. Potvin, J., Esteve, L., Brocato, B. and Peek, G.; "Experimental Study of Fluid-Structure Interactions on a Cross-Parachute: Comparison of Wind Tunnel Data and Drop Data with CFD Predictions"; 15th CEAS/AIAA Decelerator Systems Technology Conference which took place in Toulouse, France, 8-11 June 1999. AIAA Paper-99-1737.

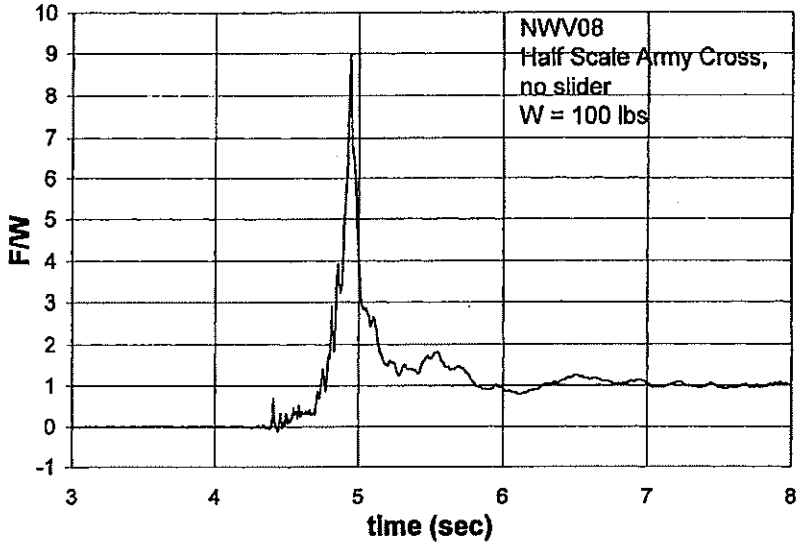

Figure 1. Typical riser loads experienced our unreefed ½-scale cruciform parachutes. The drop conditions are described in the text.

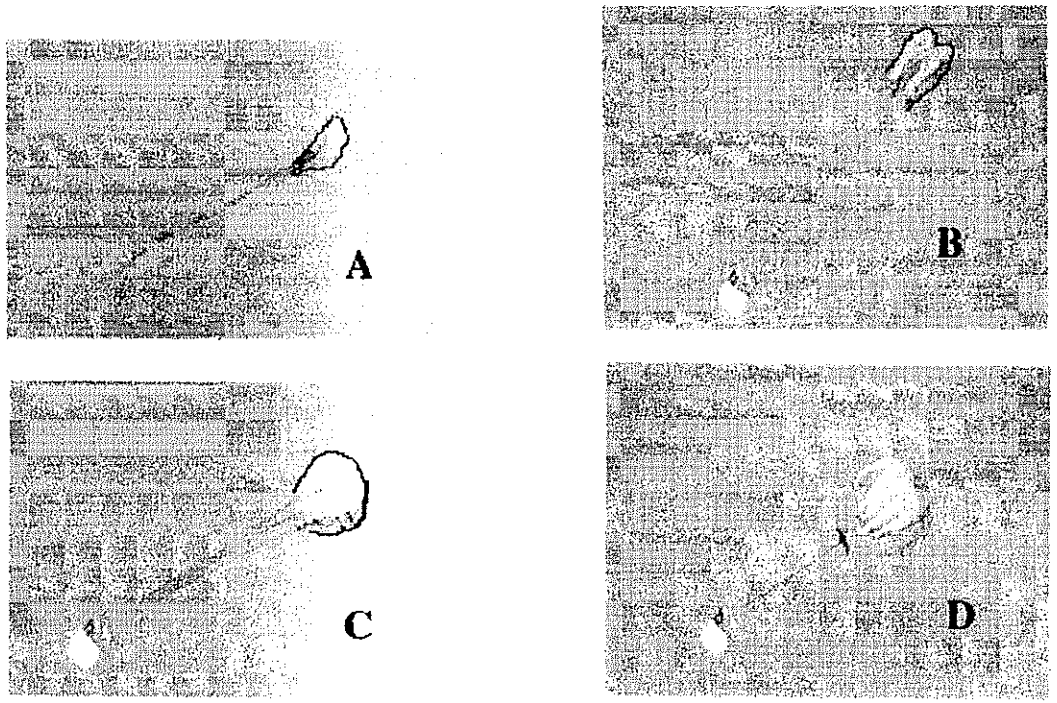

Figure 2. Opening stages of a ½-scale slider-reed cruciform parachute. Sequences (A), (B) and (C) correspond to the early pressurization stage. Figures (D) and (E) correspond to the slider descent stage.

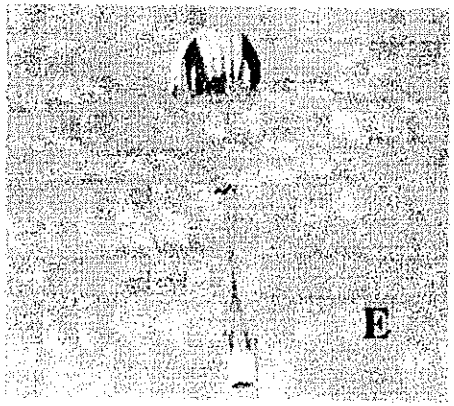

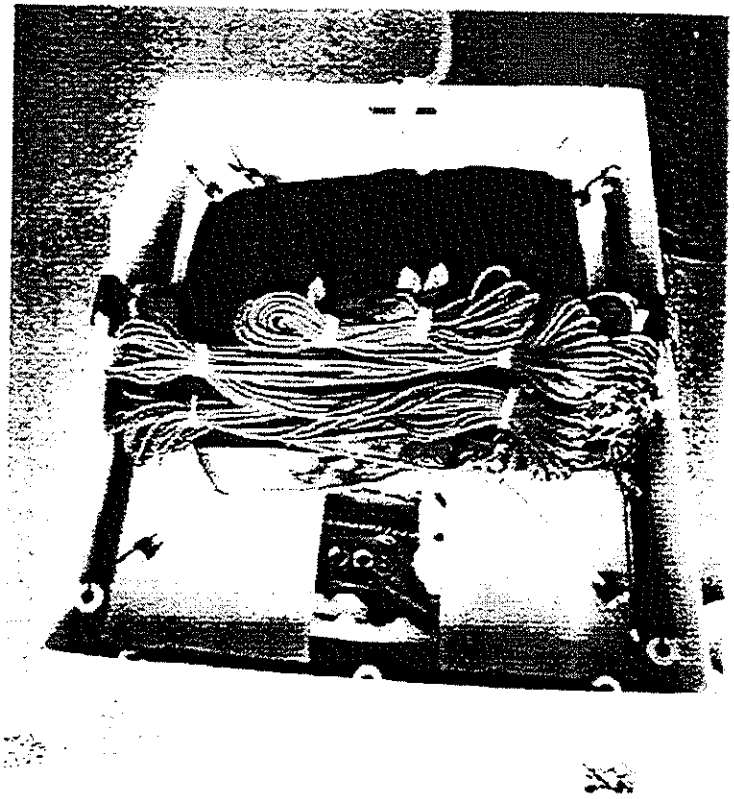

Figure 3. Top view of the payload showing the packed parachute and parts of the data acquisition system.

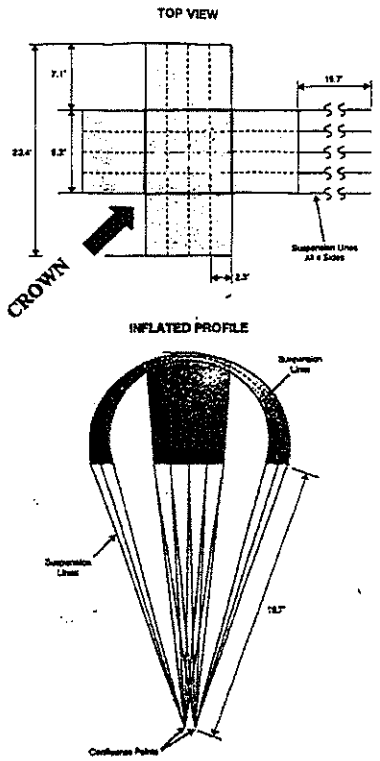

Natick, 24-Ft Cruciform Parachute (not to scale)

Figure 5. Schematics of the U.S. Army-Natick-designed test parachute used in the study.

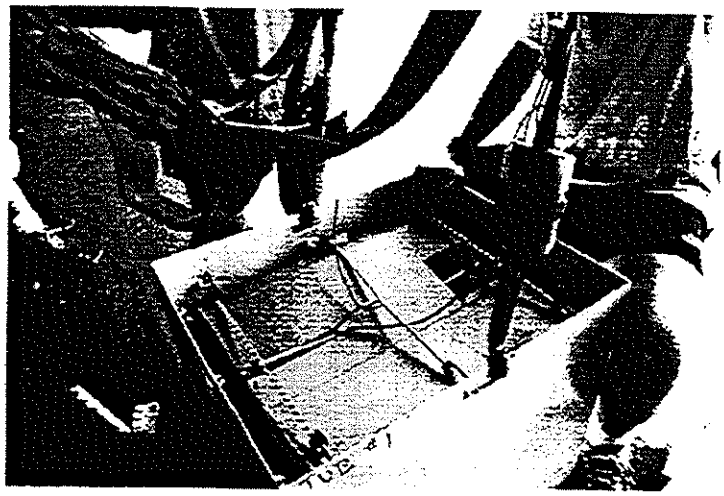

Figure 4. Top view of the payload (opened parachute configuration), showing the load cells and riser assemblies.

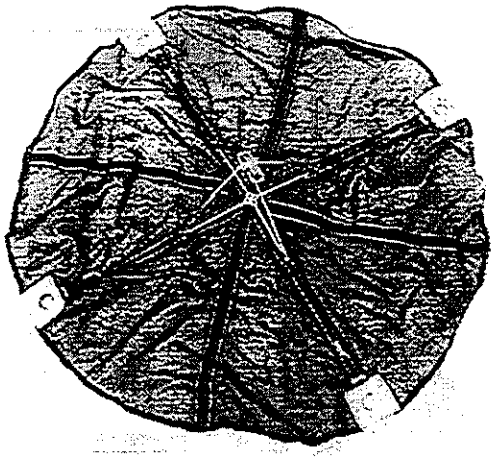

Figure 6. Early slider design used on the ½-scale parachutes. Note the spring-loaded foldable frame used to force the slider in a flat configuration. This slider had a radius of 11.5 inches.

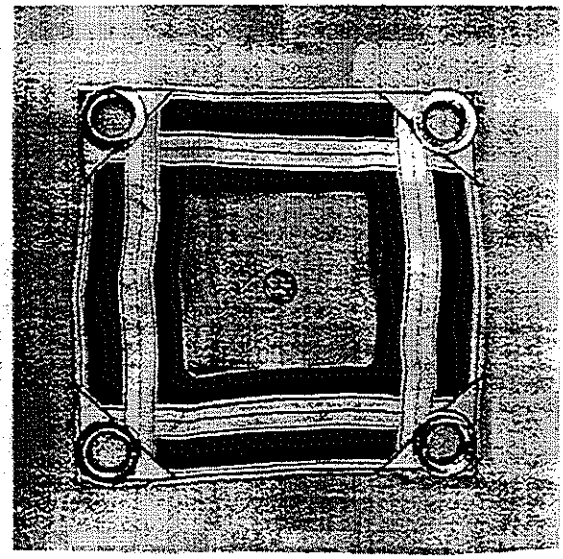

Figure 7. Smallest slider used on the full-scale parachutes. The vent dimensions are 5.5in –by- 5.5in. The outer dimensions are 1ft –by- 1ft.

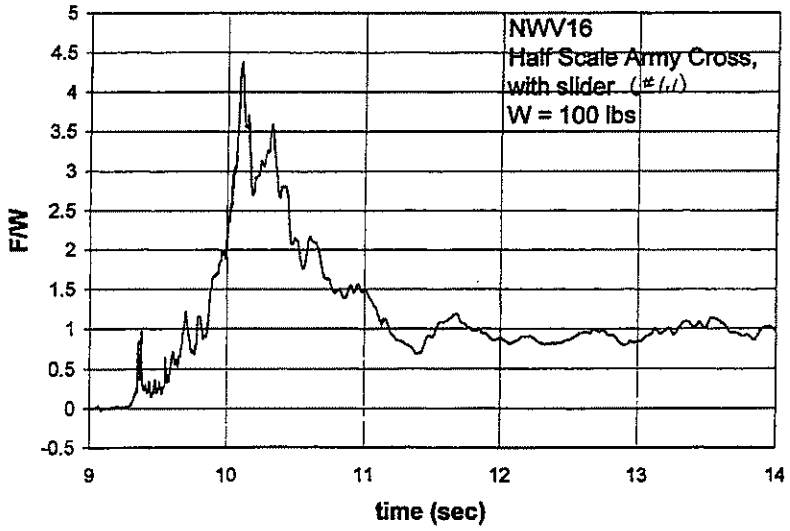

Figure 8. Typical riser loads experienced our ½-scale slider-reefed cruciform parachutes. The slider used was that shown in figure 6 but without the fabric.

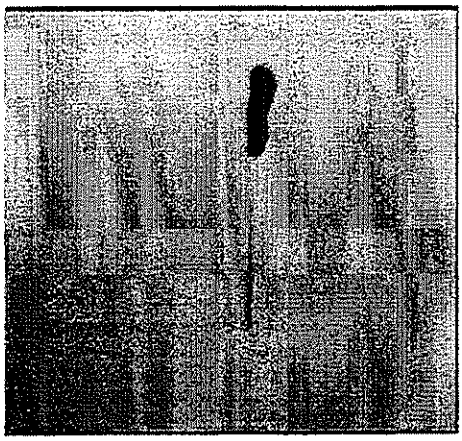

(A)

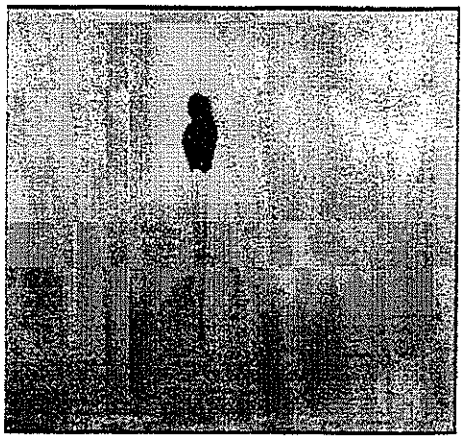

(B)

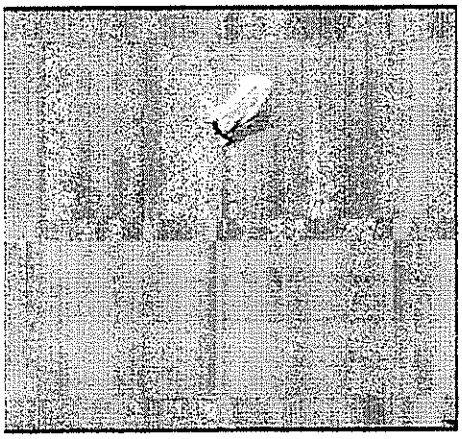

(C)

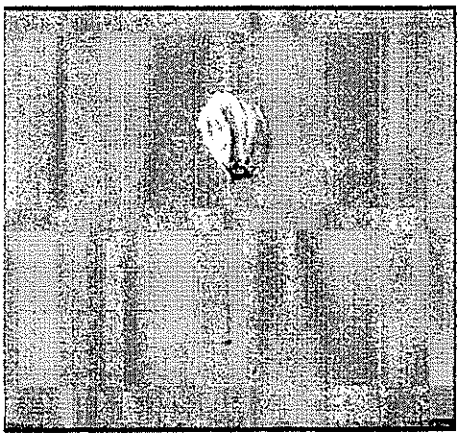

(D)

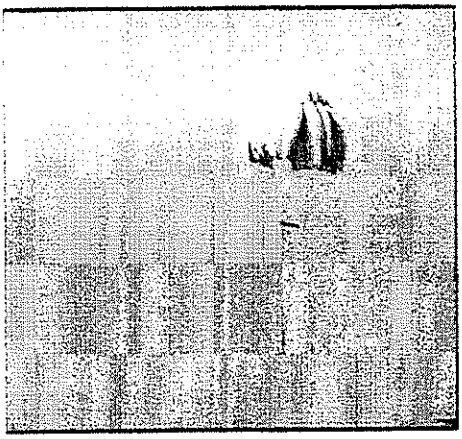

(E)

Figure 9. Slider-reefed parachutes outfitted with a reefing line around the crown, for three values of the circumference ratio $R = C_{reefline} / C_{slider}$: (A) R= 0.50; (B) R= 0.36; (C) – (D) R=1.85. (See figure 5 for definition of "crown").

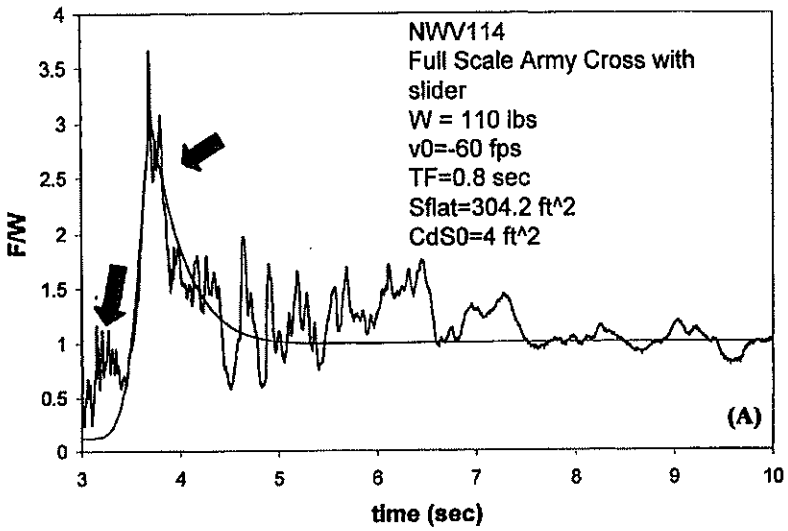

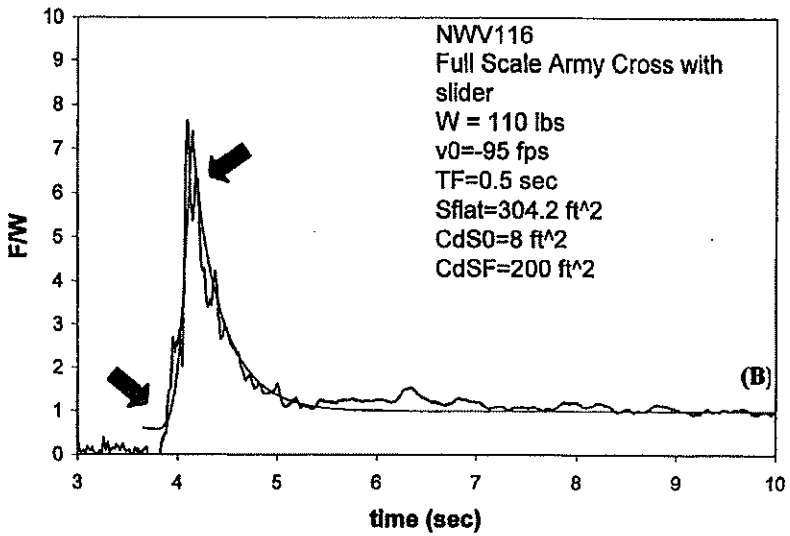

Figure 10. Theory vs. test drop data, full-scale parachute with large drag area slider. In both (A) and (B) the slider did not move substantially, keeping the parachute in a near-inverted pear shape. The two arrows show the beginning of the early pressurization and post-inflation stages.

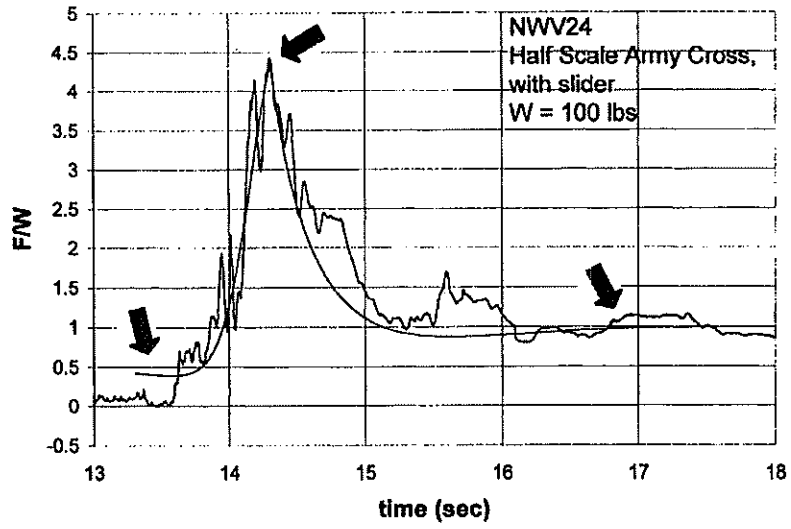

The arrows show the beginnings of the two inflation stages and of post-inflation.

Figure 11. Theory vs. test drop data, NWV24, half-scale parachute with small drag area slider (slider #1.2 in Table 1). The simulation parameters were as follows: $v(0) = 105$ ft/sec, $C_D^{steady} = 0.8$, $C_D S(0) = 4$ ft^2, $C_D S = 100$ ft^2 (@ end of early press.), $S_{flat} = 125$ ft^2, $t_{earlypress} = 1.0$ sec, and $\Gamma = 1.00$.

The arrows show the beginnings of the two inflation stages and of post-inflation.

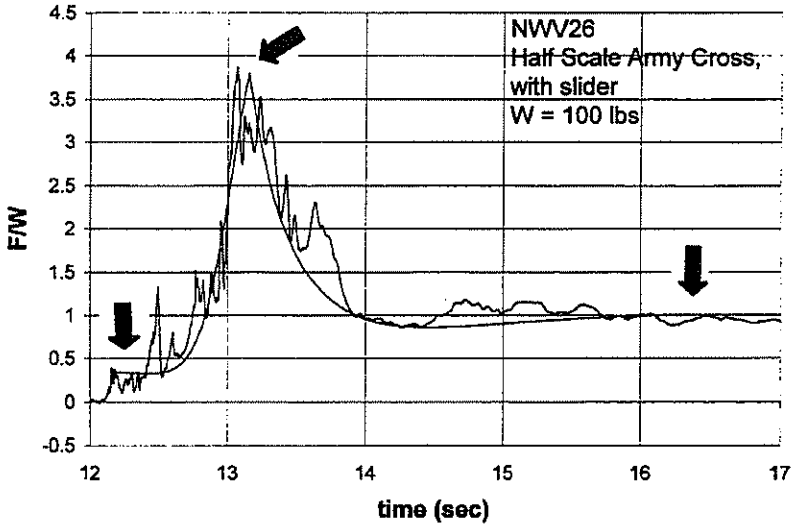

Figure 12. Theory vs. test drop data, NWV26, half-scale parachute with small drag area slider (slider #1.2 in Table 1). The simulation parameters were as follows: v(0) = 95 ft/sec, $C_D^{steady} = 0.8$, $C_D S(0) = 4$ ft^2, $C_D S = 100$ ft^2 (@ end of early press.), $S_{flat} = 125$ ft^2, $t_{earlypress} = 1.0$ sec, and $\Gamma = 1.00$.

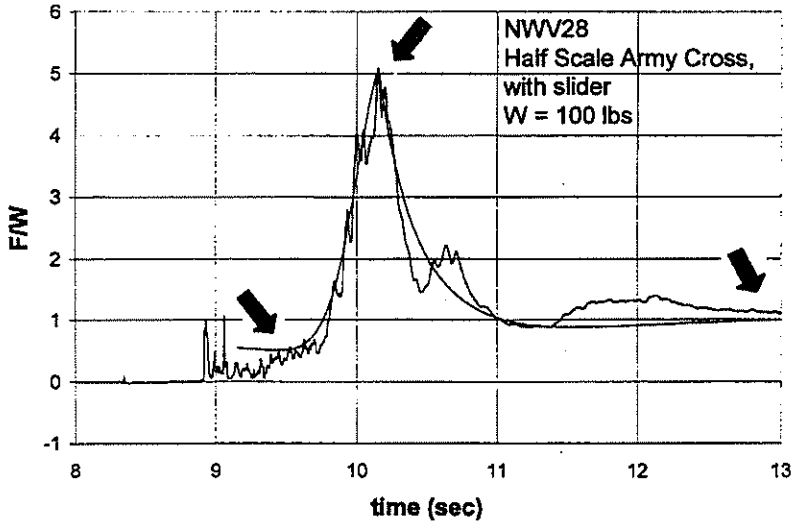

Figure 13. Theory vs. test drop data, NWV28, half-scale parachute with small drag area slider (slider #1.2 in Table 1). The simulation parameters were as follows: v(0) = 120 ft/sec, $C_D^{steady} = 0.8$, $C_D S(0) = 4$ ft^2, $C_D S = 100$ ft^2 (@ end of early press.), $S_{flat} = 125$ ft^2, $t_{earlypress} = 1.0$ sec, and $\Gamma = 1.00$.

Biased cruciform chute study: dots represent 51" suspension lines, ie standard trim.
Dots + lines represent biased lines

Configuration 1:

Cases 1: both lines shortened by 4.25" or 3.00" or 2.00" or 1.12"
Cases 2: both lines lengthened by: 5.0" or 3.0", or 2.0" or 1.25"

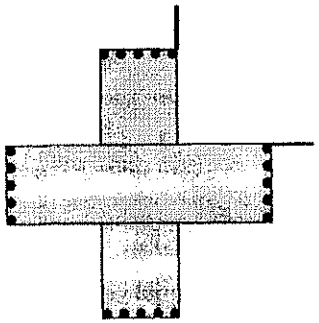

Configuration 2 :

All 4off-trim lines shortened by: 2.0" or 3.0" or 4.25"

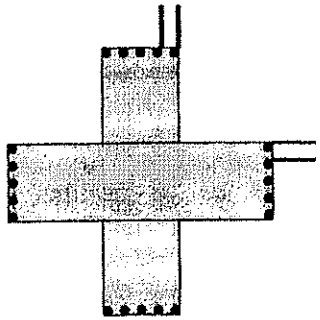

Configuration 3 :

Case 1: 4 lines off-trim by 3.0"
(shorter or longer depending on location; see diagram)

Case 2: Shorter line off-trim by 4.0"
longer lines off-trim by 3.0"

Case 3: 4 lines off-trim by 1.25"
(shorter or longer depending on location; see diagram)

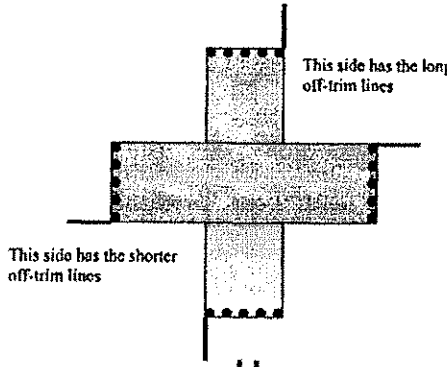

Configuration 4 :

Case 1: Shorter lines off-trim by 4.0"
Longer lines off-trim by 3.0"
Case 2: Shorter lines off-trim by 5.0"
Longer lines off-trim by 3.0"

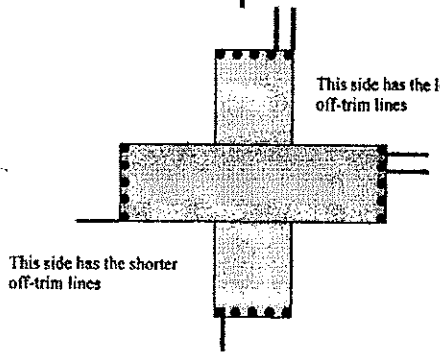

Configuration 5 :

Case 1:
Shorter lines off-trim by 5.0"
Longer lines off-trim by 3.0"

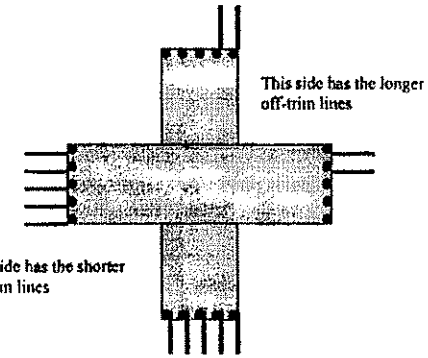

Figure 14. Line trim configurations studied in the wind tunnel. The dots correspond to suspension line attachments, and the line-dots to the lines pulled or lengthened to effect the desired glide trim.

Slider number	shape	Diameter (in)	Vent diameter (in)	% lentgh of travel down susp. lines
1.0	circular	23.0	0.0	Almost none
1.1	circular	23.0	8.0	50
1.2	circular	23.0	19.0	70-90

Table 1. List of sliders used on the ½-scale Army-Natick Cruciform parachutes.

Slider number	shape	Diameter (in)	Vent diameter (in)	% lentgh of travel down susp. lines
3.1	circular	43.0	12.0	30-50

Table 2. List of sliders used on the ½-scale C-9 parachute.

Slider number	shape	Diameter (in x in)	Circular Vent diameter (in)	% lentgh of travel down susp. lines
10	rectangular	34.24 x 35.50	8.0	Almost none
11	rectangular	34.24 x 35.50	20.0	50
12	rectangular	21.0 x 21.0	10.0	50-60
13	rectangular	12.0 x 12.0	5.50	60-70

Table 3. List of sliders used on the full-scale Army-Natick Cruciform parachutes.

Table 4a. Unreefed ½-scale cruciform

NWV drop#	F_{MAX} /W	½ peak width (sec)	Infl. + decel. time (sec)	long susp. lines short susp. lines
02	7.0	0.25	1.0	Long
08	9.0	0.12	1.5	Long
10	12.0	0.04	1.6	Long
21	8.5	0.14	0.7	Short
23	7.8	0.14	0.6	Short
25	5.5	0.60	2.0	Short
27	13.0	0.10	0.75	Short
29	7.1	0.45	1.2	Short

Table 4b. Slider-reefed ½-scale cruciform

NWV drop#	slider number	F_{MAX} /W	½ peak width (sec)	Infl. + decel. time (sec)	long susp. lines short susp. lines
14	1.1	2.5	0.60	3.5	Long
16	1.1	4.2	0.75	2.0	Long
18	1.1	3.7	1.00	3.5	Long
20	1.1	5.0	1.40	2.5	Long
22	1.2	5.0	0.75	2.0	Long
24	1.2	4.5	0.70	2.5	Long
26	1.2	3.7	0.60	1.8	Long
28	1.2	5.0	0.45	2.1	Long
31	1.1	2.7	1.20	2.1	Short
33	1.1	2.1	1.00	1.7	Short
35	1.1	2.0	2.00	2.8	Short

Table 4c. Unreefed full-scale cruciform

NWV drop#	F_{MAX}/W	½ peak width (sec)	Infl. + decel. time (sec)	remarks
102	4.6	1.0	2.7	W = 110 lbs
104	4.5	0.8	1.7	W = 110 lbs

Table 4d. Slider-reefed full-scale cruciform

NWV drop#	slider number	F_{MAX}/W	½ peak width (sec)	Infl. + decel. time (sec)	long susp. lines short susp. lines
108	10	4.5	1.0	3.0	W = 110 lbs
112	11	3.0	1.2	4.5	W = 110 lbs
114	11	3.2	0.8	4.4	W = 110 lbs
116	11	6.5	0.4	1.2	W = 110 lbs

Table 5. Configuration 1

Shortened off-trim lines – 45 mph

Force	Off-trim by 1.12in.	Off-trim by 2.00in	Off-trim by 3.00in	Off-trim by 4.25in **Slack lines seen**
Drag (lbs)	57.3	63.0	50.0	50.0
Driving (lbs)	0.53	0.76	1.62	2.85

Table 6. Configuration 2

Shortened off-trim lines - 45 mph

Force	Off-trim by 2.00in	Off-trim by 3.00in	Off-trim by 4.25in **Slack lines seen**
Drag (lbs)	52.0	51.0	46.0
Driving (lbs)	1.17	2.34	1.87

Table 7. Configuration 3

Shortened and lengthened off-trim lines - 45 mph

Force	Shorter lines off-trim by 1.25in and longer lines off-trim by 1.25in.	Shorter lines off-trim by 3.00in and longer lines off-trim by 3.00in. **Slack lines seen**	Shorter lines off-trim by 4.00in and longer lines off-trim by 3.00in. **Slack lines seen**
Drag (lbs)	56.7	50.0	43.6
Driving (lbs)	5.87	5.51	7.39

Table 8. Configuration 4

Shortened and lengthened off-trim lines - 40 mph

Force	Shorter lines off-trim by 4.00in and longer lines off-trim by 3.00in. **Slack lines seen**	Shorter lines off-trim by 5.00in and longer lines off-trim by 3.00in. **Slack lines seen**
Drag (lbs)	34.2	37.5
Driving (lbs)	6.88	8.35

Table 9. Configuration 5

Shortened and lengthened off-trim lines - 40 mph

Force	Shorter lines off-trim by 4.00in and longer lines off-trim by 3.00in.
Drag (lbs)	29.2
Driving (lbs)	7.5